Strain and temperature sensor using few-mode fiber, designing guidelines and results

Irawati, Ninik; Grüner-Nielsen, Lars; Søgaard Rishøj, Lars; Rottwitt, Karsten

Published in:
Optical Fiber Technology

Link to article, DOI:
10.1016/j.yofte.2023.103465

Publication date:
2023

Document Version
Publisher's PDF, also known as Version of record

Optical Fiber Technology 80 (2023) 103465

Contents lists available at ScienceDirect

Optical Fiber Technology

journal homepage: www.elsevier.com/locate/yofte

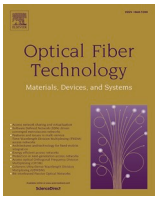

Strain and temperature sensor using few-mode fiber, designing guidelines and results

Ninik Irawati [a,*], Lars Grüner-Nielsen [a,b], Lars Søgaard Rishøj [a], Karsten Rottwitt [a]

[a] Electrical and Photonics Engineering Department, Technical University of Denmark, 2800 Kongens Lyngby, Denmark
[b] Danish Optical Fiber Innovation, 2700 Brønshøj, Denmark

ARTICLE INFO

Keywords:
Few mode fiber
Optical fiber sensors
Strain sensor
Temperature sensor

ABSTRACT

Strain and temperature sensing based on mode interference in a few-mode fiber is analyzed theoretically and experimentally. The effect of using different mode combinations is explored. A fiber guiding four LP modes is investigated as an example. Good agreement between modeling and experimental results is found for strain sensor. We demonstrate the sensors feasibility by measuring strain ranging from 0 mm to 16 mm with a sensitivity of 3.43 nm/mm and measuring temperature ranging from 30 °C to 100 °C with a sensitivity of 4.8 pm/°C.

1. Introduction

Strain sensors have a wide range of applications including measuring structural changes or mechanical deformations, studying fatigue in materials, characterizing structures, and human motions [1–3]. Likewise, temperature sensors have multiple applications in measuring the temperature of objects within medical care, agriculture, and food industry [4–6]. Combined strain and temperature sensing have attracted tremendous attention, due to versatile applications within, for example, structural health monitoring [7,8], and biomedical application [9]. The advantages of using optical fiber sensors include a small footprint, easy integration, robustness, immunity to electromagnetic fields, high sensitivity, capabilities of multiplexing, lightweight, and chemical inertness. These properties make optical fiber sensors promising candidates for strain and temperature monitoring [10,11,12]. Various types of optical fibers may be used for optical sensing, here, we investigate few-mode fibers (FMF). These add more flexibility and enhanced capabilities in comparison with more conventional single-mode fibers (SMF).

FMFs typically support up to a few tens of modes and have until now mostly been used within optical communication using the individual modes as individual data channels [13], enabled by careful control of intermodal coupling [14]. The latter makes FMF prospective candidates not only for optical communication, but also for optical sensors [15,16]. Comparing FMF with SMF, FMF has the advantage that various modes may respond differently when the fiber is exposed to the external stimulus [17] and potentially offer higher signal-to-noise ratio (SNR) levels [18]. In recent years, various types of FMF based sensors have been proposed, including sensors for temperature [15,16,19], strain [15,16,19], relative humidity [20], vibration [21], respiration monitoring [22], refractive index changes [23], and surface plasmon resonance biosensors [24].

Specifically, in relation to temperature and strain sensing, FMF based sensors have been suggested by a few groups. Zhan *et al.* [15] have proposed temperature and strain discriminative sensing based on Mach-Zehnder interferometers (MZI) in a 36.5 cm long few-mode multicore fiber. The temperature and strain sensitivities of their proposed sensor are 105.8 pm/°C and 13.96 pm/με, respectively. Lu *et al.* [16] reported strain sensitivity of − 0.013 nm/με and temperature sensitivity of −0.212 nm/°C by using a 20 cm FMF spliced in between two standard SMFs and spliced a FBG to the output SMF. In another report, temperature sensitivities of −34.3 pm/°C and 10.7 pm/°C and strain sensitivities of −2 pm/με and 0.67 pm/με, respectively, were achieved by combining 6.5 cm of FMF with a fiber Bragg grating [19]. This sensor design creates different phase-shift between individual modes due to the unique propagation constant of each mode [19].

In this paper, we investigate a simple sensor design for monitoring strain and temperature, consisting of a FMF spliced between two pieces of SMF. We denote this as a SMF-FMF-SMF (SFS) structure. The underlying operating principle of the SFS structure is interference between different modes in the FMF. The idea to use interference between two modes in a FMF for strain and temperature sensing is not new [25]. The idea to use a SFS structure for launching and detection of the two modes has been investigated by several groups [16,26,27]. However, here we present for the first time, to the best of our knowledge, a model that

* Corresponding author.
E-mail address: ninir@dtu.dk (N. Irawati).

https://doi.org/10.1016/j.yofte.2023.103465
Received 21 May 2023; Received in revised form 19 July 2023; Accepted 1 August 2023
Available online 8 August 2023

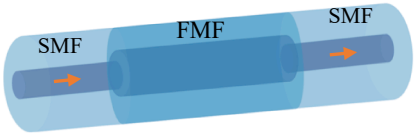

Fig. 1. Configuration of the SFS structure, the arrows indicate the direction of the sensing signal.

allows us to compare the use of different possible mode combinations. The model is confirmed by experiments. To measure the actual modes involved in the experimental investigation, we have used spatial and spectral (S^2) imaging [28,29], which allows imaging of multiple modes propagating in the fibers and to measure their relative power levels [30].

2. Methodology

A schematic of the SFS structure is presented in Fig. 1. The operating principle of the device is interference among modes in the FMF section, which is influenced by changes in external parameters, such as temperature and strain [17]. The fundamental mode that propagates in the SMF couples into the FMF and excites modes with different propagation constants. After passing through the FMF section each mode couples back to the fundamental mode of the output SMF. The modes interfere due to each having accumulated a different phase shift.

To characterize our strain and temperature sensor we conducted three types of experiments with three different experimental setups, see Fig. 2. Fig. 2(a) shows the experimental setup of the strain sensor. It consists of two pieces of SMF spliced to either end of a FMF, a tunable laser source (HP 81689A), and power meter (HP 81533B). The SFS structure is fabricated using a commercial fusion splicer, by splicing the SMF to a 1-meter-long OFS step-index four mode fiber having a 25 μm core diameter and a NA of 0.12, which supports the mode groups LP_{01}, LP_{02}, LP_{11}, and LP_{21} [29]. The FMF is clamped at two points, where one of the clamps is attached to a motorized translational stage. The function of the translation stage is to stretch the fiber in 0.05 mm steps. The transmission spectrum through the fiber was recorded from a wavelength of 1530 nm to 1570 nm in steps of 0.02 nm and the insertion loss of the sensor is 3 dB.

The schematic of the setup used for the S^2 measurement is shown in Fig. 2(b). This measurement gives information about both the power distribution between the modes and their differential group delay [30]. The light from the tunable light source is launched into the SMF and passed to the FMF. The length of the FMF in this experiment is 1.7 m, where 1 m of the FMF is fixed between the two fiber clamps, see Fig. 2 (b). The near-field distribution at the output end of the FMF is imaged on an infrared camera (Xenics Bobcat-320) at different wavelengths of the tunable light source.

The experimental setup for temperature sensing is shown in Fig. 2(c). Two SMF fiber pigtails are spliced to either end of a 1-meter-long FMF. One SMF is connected to a tunable light source and the other to a power meter. The sensing part of the FMF, with a length of 13.5 cm, is fixed to a thin aluminum foil covering the hotplate with heat resistant tape. The aluminum foil avoids thermal expansion of the hotplate to transfer to the fiber. To record the fiber temperature, the head of a thermocouple (RS Pro RS52) is placed under the heat resistant tape, close to the fiber. During the experiment the fiber was straightened to avoid bending.

In the experiment, the performance of the strain sensor was investigated for a series of fiber stretches ranging from 0 mm to 16 mm (0 με −16000 με) in steps of 0.05 mm obtained by the translation stage. The performance of the temperature sensor was investigated for a series of temperatures, ranging from 30 °C to 100 °C.

3. Theory and modeling

The principle of the SFS sensor is based on exiting and detecting two and only two of the guided modes of the FMF at the SMF-FMF interface. The fraction, which is exited/detected, is determined by the overlap integral of the (fundamental) mode of the SMF with the modes of the FMF.

The two exited modes of the FMF are assumed to have the electric fields E_1 and E_2:

$$E_1 = A_1 e^{\{i(\omega t-\beta_1 z-\varphi_1)\}} E_2 = A_2 e^{\{i(\omega t-\beta_2 z-\varphi_2)\}} \quad (1)$$

where A_i (i = 1, 2) are the amplitudes (real variables), ω the angular frequency β_i the propagation constants and φ_i the phases. As the two fields are launched simultaneously from the input SMF $\varphi_1 = \varphi_2$. The

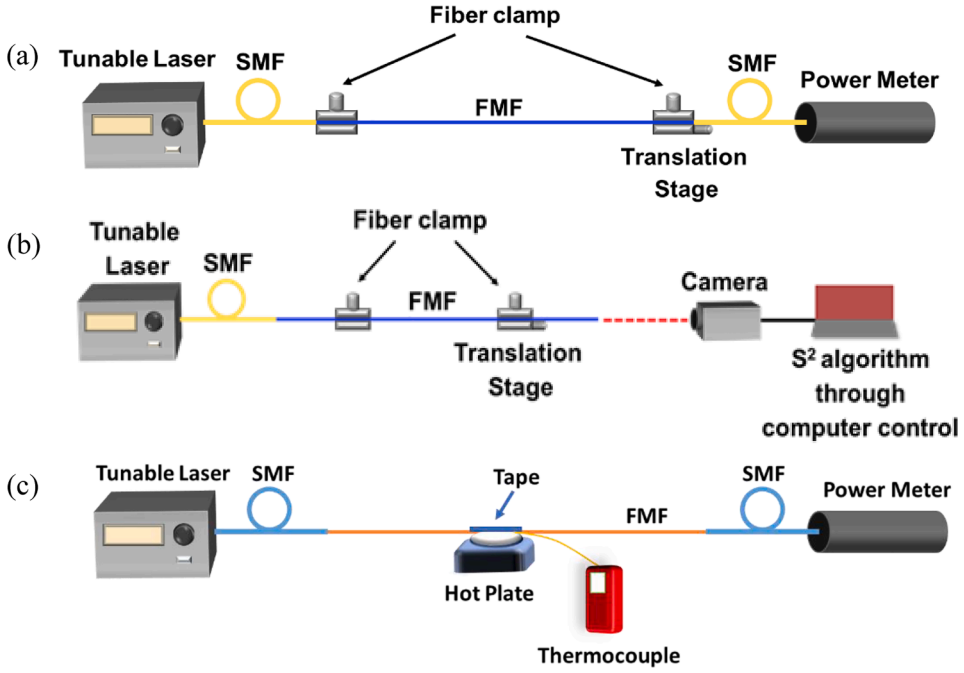

Fig. 2. Experimental setup of: (a) Strain sensor. (b) S^2 measurement for strain sensor. (c) Temperature sensor.

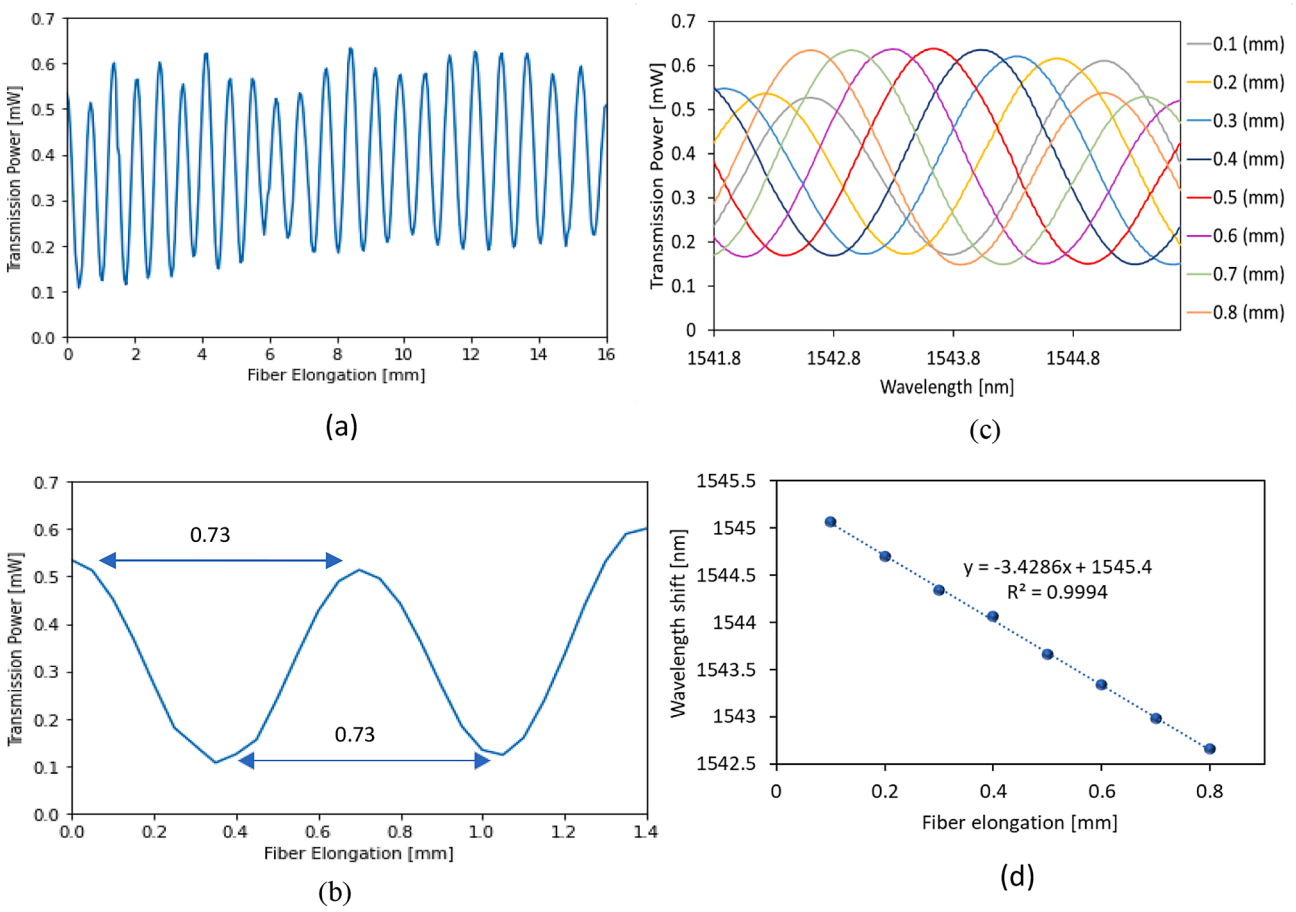

Fig. 3. Strain response. (a) Transmission power versus fiber elongation. (b) Close-up of a few oscillation periods. (c) Transmission spectra with increasing strain. (d) Wavelength shift versus strain.

power (P) in the output SMF can then be found as [30]:

$$P = P_1 + P_2 + 2A_1A_2cos(\Delta\beta L) \tag{2}$$

where $\Delta\beta = \beta_2 - \beta_1$ and the amplitudes A_i (i = 1,2) are assumed to be normalized so $P_i = E_i \cdot E_i^*$. E_i^* is the complex conjugate of E_i. It is furthermore assumed that due to the short length of FMF, the fields will be co-polarized at the output. From equation (2), the phase shift ($\Delta\beta$L) due to wavelength change is found as [30]:

$$\frac{d(\Delta\beta L)}{d\lambda} = -\frac{\Delta\tau_g L_{tot} 2\pi c}{\lambda^2} \tag{3}$$

where λ is the wavelength, $\Delta\tau_g$ is the difference in group delay (DGD) between the two modes L_{tot} is the total length of the FMF, and c is the speed of light in vacuum. From (3), it is found that the power versus wavelength vary with a period (λ_B) of:

$$\lambda_B = \frac{\lambda^2}{\Delta\tau_g \bullet L_{tot} c} \tag{4}$$

Furthermore, it can from equation (2) be observed that the amplitude of the power variation depends on the ratio of the powers in the two modes with the maximum amplitude for $P_1 = P_2$.

From equation (2) the phase shift ($\Delta\beta$L) due to strain can now be calculated:

$$\frac{d(\Delta\beta L)}{dL} = \left(\Delta\beta + \frac{d\Delta\beta}{d\varepsilon}\right)\varepsilon = \frac{\Delta L}{L_{str}} \tag{5}$$

where ε is the strain, Δ L is the elongation, and L_{str} is the length of fiber strained. From equation (5), we find that the power at a fixed wavelength vary with the fiber elongation with a period (L_B) of:

$$L_B = \frac{2\pi}{\Delta\beta + \frac{d\Delta\beta}{d\varepsilon}} \tag{6}$$

The change in propagation constant with strain can for the used step index fiber be calculated from:

$$\frac{d\Delta\beta}{d\varepsilon} = \frac{d\Delta\beta}{d\Delta n_{core}} \frac{d\Delta n_{core}}{d\varepsilon} \tag{7}$$

where Δ n_{core} is the difference between the core and cladding index.

Finally, the sensitivity in peak wavelength with change in physical length as shown in Fig. 3.c-d can be found from equation (3) and (5):

$$\frac{d\lambda_P}{d\Delta L} = -\frac{\lambda^2}{\Delta\tau_g L_{tot} 2\pi c}\left(\Delta\beta + \frac{d\Delta\beta}{d\varepsilon}\right) = -\frac{\lambda_B}{L_B} \tag{8}$$

Similarly, the effect of change in temperature (T) can be calculated. The power for a fixed wavelength will vary with temperature with a period of:

$$T_B = \frac{2\pi}{L_{heat}\left(\Delta\beta\frac{d\varepsilon}{dT} + \frac{d\Delta\beta}{dT}\right)} \frac{d\Delta\beta}{dT} = \frac{d\Delta\beta}{d\Delta n_{core}} \frac{d\Delta n_{core}}{dT} \tag{9}$$

where L_{heat} is the length of fiber being heated or cooled. The sensitivity to change in peak wavelength versus temperature is:

$$\frac{d\lambda_P}{dT} = -\frac{\lambda_B}{T_B} \tag{10}$$

To predict the sensitivities due to temperature and strain (equation (8) and (10)), we used a mode solver and the refractive index profile of

Table 1
Results for used FMF from mode solver for a wavelength of 1550 nm.

Modes		LP_{01}- LP_{11}	LP_{01}- LP_{21}	LP_{01}- LP_{02}	LP_{11}- LP_{21}	LP_{11}- LP_{02}	LP_{21}- LP_{02}
$\Delta\beta$	m^{-1}	$3.6{\cdot}10^{3}$	$8.5{\cdot}10^{3}$	$1.04{\cdot}10^{4}$	$4.9{\cdot}10^{3}$	$6.73{\cdot}10^{3}$	$1.88{\cdot}10^{3}$
$d\beta/dn_{core}$	m^{-1}	$1.34{\cdot}10^{5}$	$3.8{\cdot}10^{5}$	$6.1{\cdot}10^{5}$	$2.44{\cdot}10^{5}$	$4.73{\cdot}10^{5}$	$2.29{\cdot}10^{5}$
$\Delta\tau_g$	ps/m	2.1	4.0	3.2	1.95	1.08	0.87

Table 2
Modeling results for strain and temperature sensing using different mode combination. For a total few mode fiber length of L_{tot} = 1.0 m, a heated length of L_{heat} = 0.135 m, and a wavelength of 1550 nm.

Modes		LP_{01}- LP_{11}	LP_{01}- LP_{21}	LP_{01}- LP_{02}	LP_{11}- LP_{21}	LP_{11}- LP_{02}	LP_{21}- LP_{02}
λ_B	nm	3.81	2.00	2.50	4.11	7.42	9.20
L_B	mm	1.95	0.85	0.73	1.52	1.18	5.21
$d\lambda_P/d\,\Delta\,L$	nm/mm	−1.96	−2.35	−3.41	−2.70	−6.31	−1.77
T_B	°K	311	110	69	171	89	184
$d\lambda_P/dT$	nm/°K	$-1.2{\cdot}10^{-2}$	$-1.8{\cdot}10^{-2}$	$-3.6{\cdot}10^{-2}$	$-2.4{\cdot}10^{-2}$	$-8.4{\cdot}10^{-2}$	$-8.0{\cdot}10^{-2}$

the fibers to calculate the propagation constants and group delays for the four guided LP modes. The mode solver solves the scalar wave equation, using the finite difference method and is programmed in Python by the authors. Furthermore, the mode solver is used to determine the effect on the propagation constants due to the change in core refractive index to calculate $\frac{d\Delta\beta}{d\Delta n_{core}}$. The results for all possible mode combinations are summarized in Table 1.

The effect on Δn_{core} of a temperature change (ΔT) and strain (ε) is modeled as:

$$\Delta n_{core}(\Delta T, \varepsilon) = \Delta n_{core,0}\left(1 + \Delta T n_{Ge,T} + \varepsilon n_{Ge,S}\right) \tag{11}$$

where $\Delta n_{core,0}$ is the unperturbed Δn of the core. In [31], it is found that for a step index fiber doped with 2.9 mol% GeO_2, the thermal coefficient for the refractive index of the core is $1.15{\cdot}10^{-5}$ K^{-1}. Further, using that the thermal coefficient for the refractive index of the silica cladding is $1.06{\cdot}10^{-5}$ K^{-1} and that the GeO_2 mole% is equal to $\Delta n/1.4{\cdot}10^{-3}$ [33], we find $n_{Ge,T} = 2.2{\cdot}10^{-4}$ K^{-1}. From [32] $n_{Ge,S} = -0.587$. Further, using that $\Delta n_{core,0} = 5{\cdot}10^{-3}$ [29] we get $\frac{d\Delta n_{core}}{dT} = 1.1{\cdot}10^{-6}$ K^{-1} and $\frac{d\Delta n_{core}}{d\varepsilon} = -2.9{\cdot}10^{-3}$.

Additional, using the thermal expansion coefficient of silica of $\frac{d\varepsilon}{dT} = 0.55{\cdot}10^{-6}$ K^{-1}, the sensitives and beat length can be calculated. The results for the different mode combinations are shown in Table 2.

For a standard centered splice between the SMS and FMF, we expect to launch and detect the LP_{01} and LP_{02} of the FMF. From Table 2, it is observed that this mode combination gives the lowest value for both L_B and T_B. That is the LP_{01} and LP_{02} mode combination is the optimum. The LP_{11} and LP_{02} mode combination seems to give a higher change in peak wavelength for both temperature and strain. However as pointed out in [34] a proper figure of merit of wavelength shift based sensors is the wavelength shift sensitivity normalized with λ_B. From (8) and (10) we then find that the figure of merits are $1/L_B$ and $1/T_B$. That is the figure of merits are the highest for the LP_{01} and LP_{02} mode combination for both strain and temperature sensing.

An interesting point to note is that the ratios between strain and temperature sensitivity are not the same for the different mode combinations. E.g., the ratio is 95 °K/mm for the LP_{01}-LP_{02} mode combination and 163 °K/mm for the LP_{01}-LP_{11} mode combination. That is by measuring the wavelength shift for these two mode combinations, one will get two independent linear equations, which can be solved for temperature and strain. That is temperature and strain can be measured simultaneously. However, it will require a more advance mode launch and detection than the simple SFS structure.

4. Experimental results

To analyze the performance of the sensor, we performed a series of characterization measurements regarding temperature and strain. The experimental results for a strain measurement are presented in Fig. 3. The FMF is spliced to the SMF fibers with a standard centered splice. That is light in LP_{01} and LP_{02} modes of the FMF is launched and detected. Fig. 3(a) and Fig. 3(b) shows measured power versus fiber elongation for a wavelength of 1550 nm. The power is observed to oscillate with a

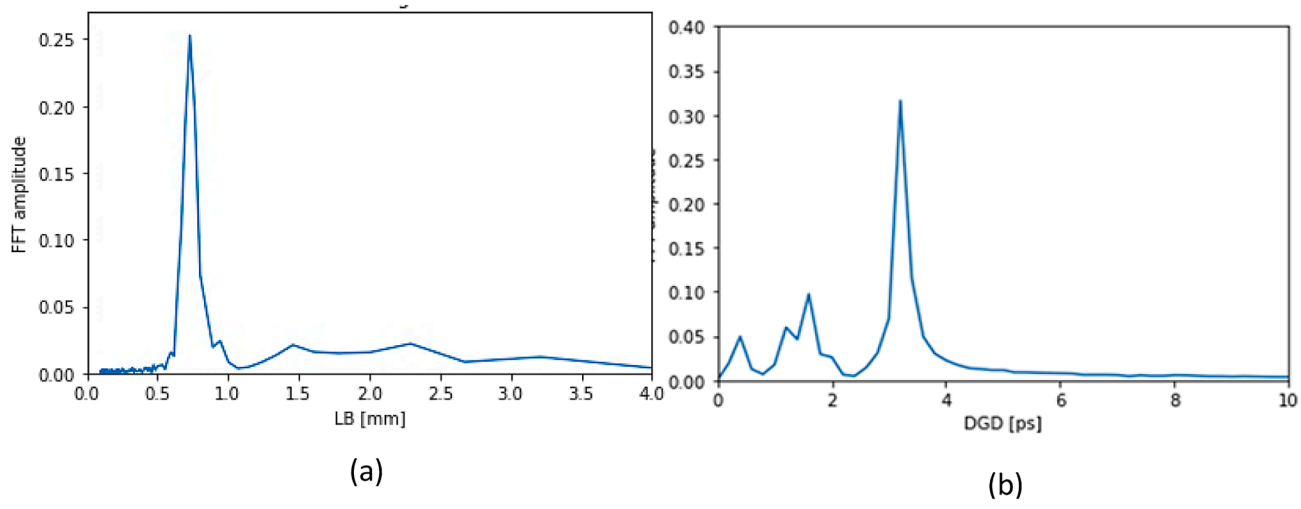

Fig. 4. The frequency spectra from Fourier transform of (a) Power vs elongation, (b) Power vs wavelength.

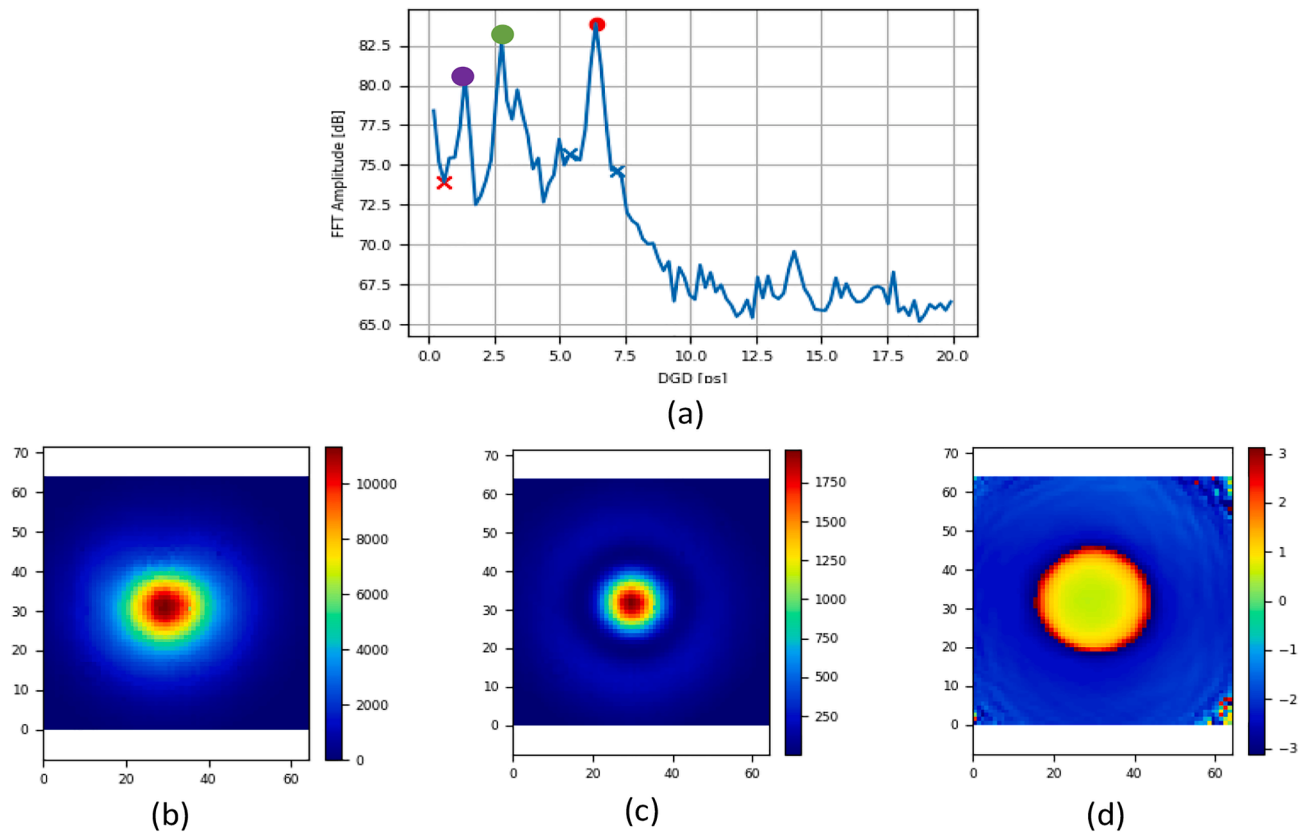

Fig. 5. S^2 measurement results for the strain sensor. (a) The sum of Fourier transforms. (b) Reconstructed intensity distribution of the dominant LP_{01} mode. (c) Reconstructed intensity distribution for the LP_{02} mode when integrating over the peak between DGD of 5.38 to 7.18 ps (blue crosses). (d) Reconstructed phase difference between the dominant mode and the LP_{02} mode at a DGD of 6.38 (red dot). (For interpretation of the references to colour in this figure legend, the reader is referred to the web version of this article.)

period of $L_B = 0.73$ mm in very good agreement with the expected theoretical value of Table 2. The change in the transmission spectrum of the sensor when the fiber was stretched from 0.1 mm to 0.8 mm is presented in Fig. 3(c). We see that the power versus wavelength oscillate with a period of $\lambda_B = 2.6$ nm. This is very close to the expected theoretical value of $\lambda_B = 2.5$ nm. The peak wavelength of the SFS structure is expected to move towards shorter wavelengths for increasing strain. In our case, it was found that the peak wavelength shifted from 1545.16 nm to 1542.66 nm, as the fiber stretch was increased from 0.05 mm to 0.8 mm, see Fig. 3(d). The experimental data fits a linear trend with a correlation coefficient of more than 0.99. This gives a measured strain sensitivity of the device of −3.43 nm/mm. This is very close to the modeled value of −3.41 nm/mm. It is noted that strain and temperature monitoring can be carried out either by evaluating the power change at the fixed wavelength or by the wavelength change of the resonance peak.

To investigate whether only the two modes, LP_{01} and LP_{02}, are interfering in the FMF, a Fourier transform of the power versus strain and the power versus wavelength measurement were taken using the Fast Fourier Transform (FFT) method by using Phyton software. The results are shown in Fig. 4. In Fig. 4(b), the DGD x-axis is calculated from λ_B using equation (3). From the theoretical DGD values of Table 1, the

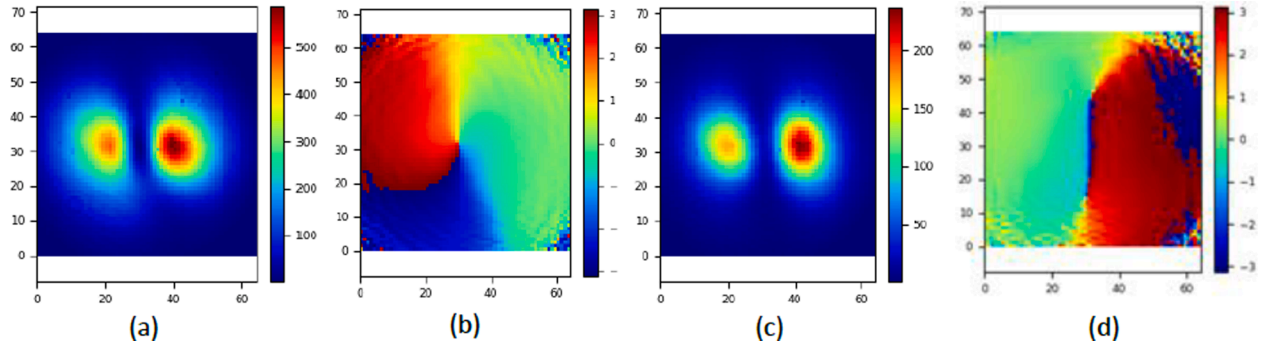

Fig. 6. S^2 measurement results for the peaks marked by the green and purple dots in Fig. 5(a). (a) Reconstructed intensity distribution of a LP_{11} mode when integrating over the peak (green dot) between DGD of 1.99 to 4.39 ps. (b) Reconstructed phase difference between the dominant mode and the LP_{11} mode at a DGD of 2.79 ps. (c) Reconstructed intensity distribution for a LP_{11} mode when integrating over the peak (purple dot) between DGD of 0.6 to 1.99 ps. (c). Reconstructed phase difference between the dominant mode and the LP_{11} mode at a DGD of 1.4 ps. (For interpretation of the references to colour in this figure legend, the reader is referred to the web version of this article.)

Table 3
Modeling against experimental results for SFS strain sensor.

Conditions			Modeling results			Measurement results			
Modes interfering	Length total m	Length under strain m	λ_B nm	L_B mm	$d\lambda/d\Delta l$ nm/mm	Mode purity launch %	λ_B nm	L_B mm	$d\lambda/d\Delta l$ nm/mm
LP_{01} - LP_{02}	3.5	1	0.72	0.73	−0.97	LP_{01}: 90 LP_{02}: 10	0.73	0.68	−1.2
LP_{01} - LP_{02}	1.75	1	1.43	0.73	−1.95	LP_{01}: 90 LP_{02}: 10	1.6	0.68	−2.4
LP_{01} - LP_{02}	1.75	0.5	1.43	0.73	−1.95	LP_{01}: 90 LP_{02}: 10	1.6	0.71	−2.3
LP_{01} - LP_{02}	0.5	0.2	5.01	0.73	−6.82	LP_{01}: 90 LP_{02}: 10	5.1	0.77	−6.5
LP_{01} - LP_{11}	1.75	1	2.18	1.95	−1.12	LP_{01}: 77 LP_{11}: 17	2.4	1.4	−1.4

dominant peak in Fig. 4(b) at 3.2 ps for a 1-meter-long fiber is therefore identified to be due to interference between the LP_{01} and LP_{02} modes, while the smaller peaks around 1.4 ps occur due to interference between the LP_{11} and LP_{01} modes, induced by the fiber clamps. In Fig. 4(a) only one peak at $L_B = 0.73$ mm is observed caused by interference between the LP_{01} and LP_{02} modes.

A S^2 measurement [30] was carried out, using the setup in Fig. 2(b), to obtain further insight regarding which modes are involved in the strain sensor. For this measurement the total fiber length was increased to 1.7 m. The S^2 measurement was taken while the fiber was elongated by 0.05 mm. A FFT of the measured power versus wavelength is performed for each camera pixel. The sum of the FFTs as a function of the DGD is shown in Fig. 5(a). Each peak in the trace arises from interference with the dominant mode, in this case, LP_{01}, and another mode. The peak value and its position relate to the relative power difference and DGD difference between the two modes, respectively. The peak at 6.4 ps (red dot) corresponds to the interference between the LP_{01} and the LP_{02} modes. The peak close to 3 ps (green dot) is due to coupling from the LP_{01} to the LP_{11} mode induced by the fiber clamp on the left-hand side of the FMF in Fig. 2(b). The peak close to 2 ps (purple dot) is similar coupling induced by the fiber clamp on the right-hand side of the FMF.

Fig. 5(b) shows the reconstructed intensity distribution of the dominant LP_{01} mode. Fig. 5(c) is the reconstructed intensity distribution when integrating over the entire peak at 6.4 ps (indicated by blue crosses in Fig. 5(a)), the relative power between these two modes is −10.4 dB. Fig. 5(d) shows the relative phase difference between these two modes, and as expected a pi-phase shift is observed along the radial direction.

The S^2 measurement corresponding to the green and purple dots in Fig. 5(a) is presented in Fig. 6. Fig. 6(a) shows the reconstructed intensity distribution integrated over the peak marked with the green dot, and Fig. 6(b) shows the phase difference of this mode relative to the dominant mode. The mode is identified as LP_{11} and its relative power compared to the dominant mode is calculated to be −11.6 dB. Fig. 6(c) shows the reconstructed intensity distribution integrated over the peak marked with the purple dot, and Fig. 6(d) shows the phase difference of this mode relative to the dominant mode. The mode is also identified as LP_{11} and its relative power compared to the dominant mode is calculated to be −16.6 dB. Based on the DGDs of these modes and measured fiber lengths it is concluded that the peaks marked by the green and purple dots arise from mode coupling induced by the left and right-hand fiber clamps acting on the FMF, respectively. Furthermore, when the tension applied to either of the fiber clamp were removed, the corresponding peak disappeared.

In the SFS fiber sensor it is desirable to only have interference between two modes since it increases the signal-to-noise ratio of the collected data. Based on the S^2 measurement it is found that the SMF to FMF splice leads to clean excitation of around 90 % of the power in LP_{01} mode and 10 % in LP_{02} mode. Care must be taken to avoid unwanted coupling to other modes, e.g., by the fiber clamps. However, the LP_{11} mode is an asymmetric mode, thus it does not couple back to the fundamental mode at the splice between the FMF and the SMF. Hence, the coupling between the LP_{11} mode and the fundamental mode is not critical for the performance of the fiber sensor.

To further verify our modeling, strain sensing experiments were performed using different length and mode combinations. The results are summarized in Table 3. Four different experimental conditions are applied for beating between the LP_{01} and the LP_{02} mode with simple splices at both end the fiber and three different total lengths. As expected, it is observed that the wavelength beat period λ_B and the sensitivity of the wavelength shift versus elongation are both inversely proportional to the total length of the FMF. The experimental results are in general in good agreement with the modeling results.

In addition, we measured the beating between LP_{01} and LP_{11} by using offset splices at both ends of the FMF. S^2 measurement showed that 77% of the power is in the LP_{01} mode and 17% is in the LP_{11} mode with a small amount of power in the other modes. Also, for this mode combination there is a reasonable agreement between modeling and measurements. The agreement is not quite as good as for the LP_{01} and LP_{02} mode combination, most likely due to disturbance from the other exited modes.

Finally, the temperature dependence of the SFS sensor (using standard splices between SMF and FMF) was investigated by increasing the temperature from 30 °C to 100 °C in steps of 5 °C. Fig. 7(a) shows the measured transmission spectra, where the resonance peak is observed to

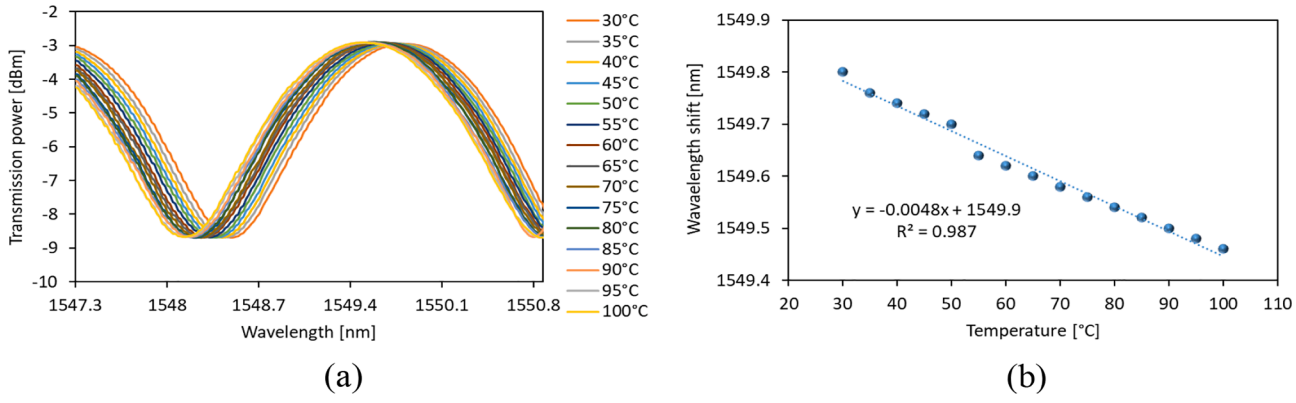

Fig. 7. (a) Transmission spectra of the SFS sensor for different temperatures. (b) Wavelength shift as a function of temperature.

shift from 1549.80 nm to 1549.46 nm as the temperature is increased. Fig. 7(b) shows the shift of the resonance peak, along with a linear fit. The linear correlation coefficient is 0.987 and the slope is −4.8 pm/°C. This value is numerically much lower than the modeled value of −36 pm/°C. An explanation for this deviation might be that our modeling overestimates the thermo-optic effect. Consequently, we expect that the used value for $n_{Ge,S}$ is too large.

5. Conclusion

We have reported a single mode – few mode – single mode (SFS) fiber structure for strain and temperature sensing using a simple, compact, and cost-effective design. For the strain sensor, a very good agreement between modeling and measurements was obtained. For the temperature sensor the model did not agree so well with experiments. This might be due to that the used value for the thermo-optic effect on the refractive index of germanium doped silica was too high. It is found that the mode combination of LP_{01} and LP_{02} obtained in a SFS using a standard splice is the optimum giving highest sensitivity for both strain and temperature sensing.

Our simulations indicate that by using two sets of mode combinations, it will be possible to discriminate between temperature and strain. However, it will require a more advanced mode launch and mode detection scheme than the current SFS structure.

Declaration of Competing Interest

The authors declare that they have no known competing financial interests or personal relationships that could have appeared to influence the work reported in this paper.

Data availability

Data will be made available on request.

Acknowledgment

This work was supported by Independent Research Fund Denmark in grant 1032-00260B, VOLTOFI.

References

[1] Güemes, A. Fernández-López, P.F. Díaz-Maroto, A. Lozano, J. Sierra-Perez, Structural health monitoring in composite structures by fiber-optic sensors, Sensors 18(4) (2018) 1094.
[2] T. Yamada, Y. Hayamizu, Y. Yamamoto, Y. Yomogida, A. Izadi-Najafabadi, D. N. Futaba, K. Hata, A stretchable carbon nanotube strain sensor for human-motion detection, Nat. Nanotechnol. 6 (2011) 296–301.
[3] V.E. Zetterlind, S.E. Watkins, M.W. Spoltman, Fatigue testing of a composite propeller blade using fiber-optic strain sensors, IEEE Sens. J. 3 (4) (2003) 393–399.
[4] R. Correia, S. James, S.-W. Lee, S.P. Morgan, S. Korposh, Biomedical application of optical fibre sensors, J. Opt. 20 (7) (2018) 073003.
[5] M.E.E. Alahi, L. Xie, S. Mukhopadhyay, L. Burkitt, A temperature compensated smart nitrate-sensor for agricultural industry, IEEE Trans. Ind. Electron. 64 (9) (2017) 7333–7341.
[6] R. Vadivambal, D.S. Jayas, Applications of thermal imaging in agriculture and food industry—a review, Food Bioprocess Technol. 4 (2) (2011) 186–199.
[7] G. Laffont, R. Cotillard, N. Roussel, R. Desmarchelier, S. Rougeault, Temperature resistant fiber Bragg gratings for on-line and structural health monitoring of the next-generation of nuclear reactors, Sensors 18 (6) (2018) 1791.
[8] J. Braunfelds, U. Senkans, P. Skels, R. Janeliukstis, T. Salgals, D. Redka, I. Lyashuk, J. Porins, S. Spolitis, V. Haritonovs, V. Bobrovs, C. Riziotis, FBG-based sensing for structural health monitoring of road infrastructure, J. Sens. 2021 (2021) 1–11.
[9] P. Roriz, S. Silva, O. Frazão, S. Novais, Optical fiber temperature sensors and their biomedical applications, Sensors 20 (7) (2020) 2113.
[10] W. Talataisong, R. Ismaeel, G. Brambilla, A review of microfiber-based temperature sensors, Sensors 18 (2) (2018) 461.
[11] L. Fan, Y. Bao, Review of fiber optic sensors for corrosion monitoring in reinforced concrete, Cem. Concr. Compos. 120 (2021), 104029.
[12] H. Zhang, M. Zhang, J. Kang, X. Zhang, J. Yang, High sensitivity fiber-optic strain sensor based on modified microfiber-assisted open-cavity Mach-Zehnder interferometer, J. Lightwave Technol. 39 (13) (2021) 4556–4563.
[13] K.I. Kitayama, N.P. Diamantopoulos, Few-mode optical fibers: Original motivation and recent progress, IEEE Commun. Mag. 55 (8) (2017) 163–169.
[14] P. Sillard, M. Bigot-Astruc, D. Molin, Few-mode fibers for mode-division-multiplexed systems, J. Lightwave Technol. 32 (16) (2014) 2824–2829.
[15] X. Zhan, et al., Few-mode multicore fiber enabled integrated Mach-Zehnder interferometers for temperature and strain discrimination, Opt. Express 26 (12) (2018) 15332–15342.
[16] C. Lu, J. Su, X. Dong, T. Sun, K.T. Grattan, Simultaneous measurement of strain and temperature with a few-mode fiber-based sensor, J. Lightwave Technol. 36 (13) (2018) 2796–2802.
[17] Y. Weng, E. Ip, Z. Pan, T. Wang, Single-end simultaneous temperature and strain sensing techniques based on Brillouin optical time domain reflectometry in few-mode fibers, Opt. Express 23 (7) (2015) 9024–9039.
[18] I. Ashry, Y. Mao, A. Trichili, B. Wang, T.K. Ng, M.-S. Alouini, B.S. Ooi, A review of using few-mode fibers for optical sensing, IEEE Access 8 (2020) 179592–179605.
[19] X. Gao, et al., A dual-parameter fiber sensor based on few-mode fiber and fiber Bragg grating for strain and temperature sensing, Opt. Commun. 454 (2020), 124441.
[20] A.D.D. Le, Y.G. Han, Relative humidity sensor based on a few-mode microfiber knot resonator by mitigating the group index difference of a few-mode microfiber, J. Lightwave Technol. 36 (4) (2018) 904–909.
[21] K.A. Yablochkin, M.V. Dashkov, Study of the vibration detection using few-mode optical fiber, in: Optical Technologies for Telecommunications 2019 11516 (2020) 115160Y.
[22] R. Wang, J. Zhao, Y.e. Sun, H. Yu, N. Zhou, H. Zhang, D. Jia, Wearable respiration monitoring using an in-line few-mode fiber Mach-Zehnder interferometric sensor, Biomed. Opt. Express 11 (1) (2020) 316.
[23] C. Lu, X. Dong, J. Su, Detection of refractive index change from the critical wavelength of an etched few mode fiber, J. Lightwave Technol. 35 (13) (Jul. 2017) 2593–2597.
[24] J. Dong, et al., Side-polished few-mode fiber based surface plasmon resonance biosensor, Opt. Express 27 (8) (2019) 11348–11360.
[25] T.A. Eftimov, W.J. Bock, Sensing with a LP_{01}-LP_{02} intermodal interferometer, J. Lightwave Technol. 11 (12) (1993) 2150–2156.
[26] E. Salik, M. Medrano, G. Cohoon, J. Miller, C. Boyter, J. Koh, SMS fiber sensor utilizing a few-mode fiber exhibits critical wavelength behavior, IEEE Photon. Technol. Lett. 24 (7) (2012) 593–595.
[27] K. Nakajima, T. Sakamoto, Y. Goto, C. Fukai, T. Matsui, et al., Study of few-mode fiber based SMS sensor for simultaneous measurement of temperature and strain, in: Proc. SPIE 9634, 24th International Conference on Optical Fibre Sensors., vol. 96343M, Sep. 2015.
[28] J.W. Nicholson, A.D. Yablon, J.M. Fini, M.D. Mermelstein, Measuring the modal content of large-mode-area fibers, IEEE J Sel. Topics. Quant. Electron. 15 (1) (2009) 61–70.
[29] K. Jespersen et al., Measuring distributed mode scattering in long, few-moded fibers, in: Optical Fiber Communication Conference, Oth3I-4, March. 2012.
[30] L. Grüner-Nielsen, N.M. Mathew, K. Rottwitt, Characterization of few mode fibers and devices, Opt. Fiber Technol. 52 (2019), 101972.
[31] Y.-J. Kim, U.-C. Paek, B.H. Lee, Measurement of refractive-index variation with temperature by use of long-period fiber gratings, Opt. Lett. 27 (15) (2022) 7233–7243.
[32] E.M. Dianov, V.M. Mashinsky, Germania-based core optical fibers, J. Lightwave Technol. 23 (11) (2005) 3500–3508.
[33] R. Olshansky, Propagation in glass waveguides, Rev. Modern Phys. 51 (2) (1979) 341–367.
[34] C. Caucheteur, T. Guo, J. Albert, Review of plasmonic fiber optic biochemical sensors: improving the limit of detection, Anal. Bioanal. Chem. 407 (14) (2015.) 3883–3897.